ELSEVIER

Journal of Structural Geology 29 (2007) 787–801

JOURNAL OF STRUCTURAL GEOLOGY

www.elsevier.com/locate/jsg

# Influence of viscosity contrast and anisotropy on strain accommodation in competent layers

Noel C. Toimil [a,*], Albert Griera [b]

[a] School of Earth, Ocean and Planetary Sciences, University of Cardiff, Park Place, Cardiff CF10 3YE, UK
[b] Departament de Geologia, Universitat Autònoma de Barcelona, 08193 Barcelona, Spain

Received 26 May 2006; received in revised form 14 November 2006; accepted 1 December 2006
Available online 30 January 2007

**Abstract**

Folds with different values of viscosity contrast and anisotropy have been simulated using the finite-difference code FLAC™. The kinematical analysis of these folds has enabled conclusions to be reached about strain accommodation mechanisms. The sequence of strain patterns in all the folds analysed only differs in the intensities of the different mechanisms involved, which depend on the mechanical properties of the folds. The order of the different strain patterns in the sequence is the same, regardless of the anisotropy and viscosity contrast. Strain accommodation in folds follows the patterns of tangential longitudinal strain, flexural flow and layer shortening. Nevertheless, no combination of these strain patterns can explain the shape of the folded layer at the inflection point and the high strain intensity values in the inner arc. These problems can only be solved by considering a variant of longitudinal tangential strain that is less intense than has classically been thought and combined with a heterogeneous distribution of flexural flow and layer shortening across the layer. The dependence of the different folding mechanisms on the mechanical properties has been used to devise a graphical method for estimating viscosity contrast and anisotropy from the intensities of the strain patterns in the sequence.


*Keywords:* Strain pattern; Folding; Strain; Kinematics

## 1. Introduction

Folds are manifestations of the heterogeneous deformation of layered rocks. In principle, there are many ways to accommodate and distribute the strain within the folded layers, and each can be achieved by following many different paths (Ramsay, 1967, pp. 343–344). However, experimental and field evidence shows that these patterns and evolutionary paths do not all have the same probability of occurring; and that folds are mainly the result of a combination of a limited number of folding mechanisms or strain patterns. Kinematical analysis of folds involves the study of these folding mechanisms, their characteristics and their evolution throughout the folding process. This represents one of the most important aims in Structural Geology, since kinematical knowledge helps in the construction of balanced cross sections, which have practical applications and are important in understanding geological history.

Kuenen and de Sitter (1938); Billings (1954, pp. 88–92), Ramberg (1961); Carey (1962); Donath (1962); Ramsay (1962); de Sitter (1964); Donath and Parker (1964) and Mukhopadhyay (1965), among others, were pioneers in research into folding mechanisms. Later, Ramsay (1967, pp. 391–436) tackled the analysis of the geometric relationships that govern the displacements of particles within a layer when it is folded by the mechanisms of tangential longitudinal strain, flexural flow and homogeneous deformation. Ramsay and Huber (1987, pp. 445–473) studied the strain magnitude and the orientation of the finite strain ellipse associated with flexural flow and with a combination of flexural flow and homogeneous deformation. They introduced the term ‘‘inverse

* Corresponding author. Present address: HUNOSA mining company, Pozo San Nicolás, 33650 Ablaña, Asturias, Sapin. Tel.: +34 985 44 61 67/76 60 00; fax: +34 985 44 61 48/76 72 05.
*E-mail address:* noelcanto@hunosa.es (N.C. Toimil).

0191-8141/$ - see front matter © 2006 Elsevier Ltd. All rights reserved.
doi:10.1016/j.jsg.2006.12.001

tangential longitudinal strain'' to refer to a strain pattern that is complementary to tangential longitudinal strain and related to the folding of incompetent material. Twiss and Moores (1992) showed examples of strain distribution in layers where the deformation was accommodated by tangential longitudinal strain, flexural flow and initial homogeneous deformation, in folds developed by bending and buckling. Bobillo-Ares et al. (2000) studied the shape of the folded layer and the strain distribution associated with tangential longitudinal strain, and analysed the problems that this mechanism presents. Bastida et al. (2003) and Bobillo-Ares et al. (2004) developed a mathematical model of tangential longitudinal strain, flexural flow and irrotational deformation by incorporating this theory in a computer program. Ormand and Hudleston (2003) studied the folding kinematics of natural folds in the Appalachian Valley-and-Ridge province. Aspects such as decrease in area and the migration of the neutral line, which affect the way in which the folded layers accommodate deformation, have been treated by Gairola (1978); Hudleston and Holst (1984); Hudleston et al. (1988); Ramsay and Huber (1987, pp. 460–461), Hudleston and Lan (1993) and Lan and Hudleston (1995).

In this paper, we constructed elastoviscous models of folds with different values of viscosity contrast and anisotropy using the *Fast Lagrangian Analysis of Continua* (FLAC™) program (Itasca Consulting Group, Inc., 1998). We then analysed the kinematical characteristics of these models with the *FoldModeler* program (Bobillo-Ares et al., 2004) developed in the MATHEMATICA™ environment. The aim was to determine the characteristics of the different folding mechanisms in the operation, such as their relative importance during the folding process and the order in which they operate. We also studied possible solutions for certain geometrical problems that arose during the analysis of the folds. Furthermore, the knowledge of the mechanical properties (viscosity contrast and anisotropy) enables the relative proportion of the different strain patterns to be related to the rheological characteristics of the layer. As a starting point, we considered the strain patterns of tangential longitudinal strain, flexural flow and irrotational homogeneous deformation, because these mechanisms represent, a priori, the most common forms of strain accommodation in isolated folded competent layers. We should remember, however, that the strain patterns considered in the folding analysis are not necessarily exclusive, and that there could be other mechanisms that account for the geometrical and kinematical characteristics of the folds better.

The kinematical study of these simulated folds is an essential prerequisite for subsequent kinematical analysis of natural folds.

## 2. Numerical modelling

The folding of a competent layer embedded in a softer matrix has been studied (Fig. 1a) using a numerical approach based on the commercial explicit finite-difference code FLAC™ (Itasca Consulting Group Inc., 1998). This code solves the discretized equations of motion using a time-marching dynamic relaxation scheme in which the inertial terms are used to reach the

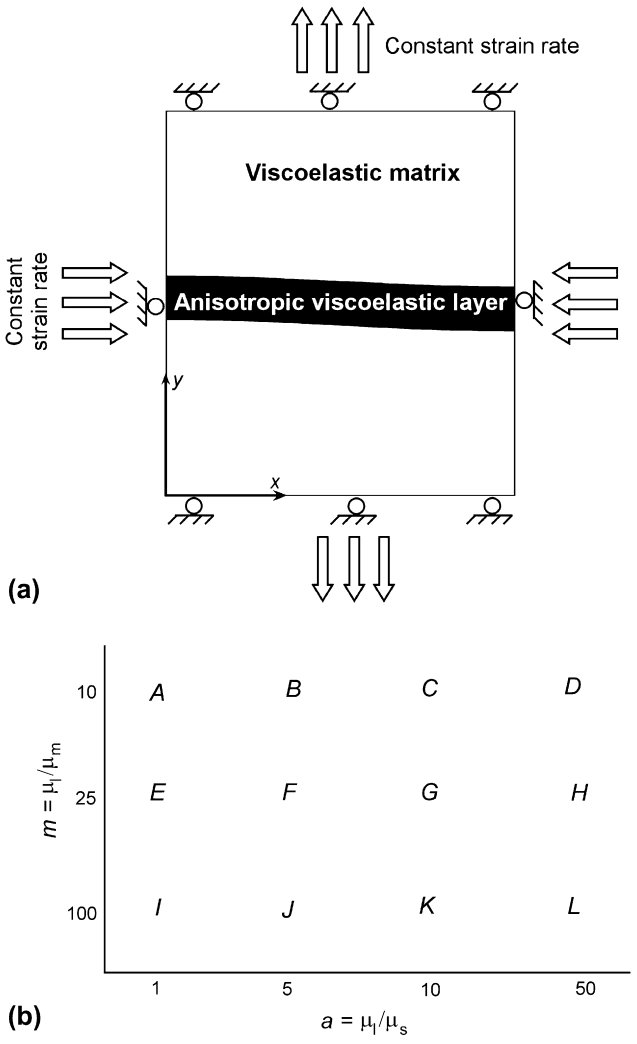


Fig. 1. (a) Initial geometry and boundary conditions of viscoelastic folding in pure shear (see text and Table 1 for details). (b) Representation of the folds (labels A to L) developed with FLAC in a diagram of anisotropy ($a$) vs. viscosity contrast ($m$).

equilibrium state. The continuum medium is divided into a finite difference grid composed of linear quadrilateral plane-strain elements. Internally, each element is divided into two superposed sets of constant-strain triangles for efficient handling of volumetric constraints. A mixed discretization scheme is used to prevent ''hourglassing'' or ''mesh-locking'' problems (Marti and Cundall, 1982). The code has previously been used to investigate a wide range of deformation processes relevant to structural geology (i.e. Hobbs et al., 1990; Ord, 1990; Zhang et al., 1996; Passchier and Druguet, 2002; Takeda and Griera, 2006).

A linear elasto-viscous (Maxwell) material model was adopted (Turcotte and Schubert, 1982). According to this rheology, the strain rate is the superposition of a linear elastic strain rate and a linear viscous strain rate. For a reference frame parallel to the layer, the compliance between the deviatoric strain rate ($\dot{\varepsilon}$) and stress ($\tau$) can be expressed as,

$$\dot{\varepsilon}_{ij} = \frac{1}{2G}\dot{\tau}_{ij} + \frac{1}{2\mu_{ij}}\tau_{ij} \qquad (1)$$

where $G$ and $\mu$ are the elastic shear modulus and the coefficient of viscosity, respectively. The viscous response of the stiffer layer was considered anisotropic, while elastic properties and matrix viscosity were considered isotropic. The anisotropic material is fully defined using two different components: normal viscosity ($\mu_l$, for $i = j$) and shear viscosity ($\mu_s$, for $i \neq j$). Normal viscosity describes the resistances of the layer to normal stresses, and will be the viscosity of the layer if the material is isotropic, whereas the shear coefficient represents the resistance to simple shear within the layer. It is fulfilled that $\mu_l \geq \mu_s$. Thus, when $\mu_l = \mu_s$, the material is isotropic, and as $\mu_s$ decreases with respect to $\mu_l$, the anisotropy of the material increases (Johnson and Fletcher, 1994, pp. 419–424; Hudleston et al., 1996). The viscosity contrast is defined as $m = \mu_l/\mu_m$ ($\mu_m$ being the viscosity of the incompetent matrix) and the anisotropy of the layer as $a = \mu_1/\mu_s$. Therefore, the shear viscosity can be expressed as $\mu_s = \mu_m m/a$. Values of elastic and viscous properties used are listed in Table 1, and are similar to those used for previous numerical studies of folding (Mancktelow, 1999). These values are in agreement with the range established for natural rocks (Turcotte and Schubert, 1982). The range of Deborah numbers employed in the present simulations is $10^{-3}$ to $10^{-6}$ and is close to that expected for viscous behaviour (Poliakov et al., 1993). On the other hand, compressibility of the material is considered purely elastic and the bulk modulus ($K$) is taken as $2 \times 10^{10}$ Pa. The area variation at the end of the simulations does not reach 1%.

The geometry of the model consists of a central layer of two units of thickness, positioned in parallel to the compression axis. A constant initial sinusoidal perturbation has been assigned for all the models with an initial amplitude of 0.1 and wavelength to layer thickness of 16. This closely corresponds to the theoretical dominant wavelength/thickness ratio for a viscosity contrast of 100 (Johnson and Fletcher, 1994, p. 209). Considering the symmetry of the problem, only one half wavelength of the fold has been modelled. We used a total of 768 quadrilateral elements to define the mesh; the layer width was represented by 8 elements and the length by 24 elements.

Progressive shortening parallel to the layer was achieved by means of velocity boundary conditions at a constant strain rate of $2 \times 10^{-14}$ s$^{-1}$. The normal velocity component on the convergent sides (left and right) was prescribed, while parallel and convergent on other sides (upper and lower) were unconstrained. A coherent boundary between competent layer and matrix is assumed and slip is not allowed to occur.

Table 1
Material properties of the models developed with FLAC

| | | |
|---|---|---|
| Geometrical properties | Geometry of the initial perturbation | Sinusoidal |
| | Wavelength to thickness (length/thickness) | 16 |
| | Normalized amplitude ($h = y/x$) of the initial perturbation | 0.0125 |
| | Shear modulus ($G$) | $1 \times 10^{10}$ Pa |
| Elastic properties | Bulk modulus ($K$) | $2 \times 10^{10}$ Pa |
| | Range of normal viscosity ($\mu_l$) | $1 \times 10^{20}$–$1 \times 10^{21}$ Pa s |
| Viscosity properties | Range of shear viscosity ($\mu_s$) | $2 \times 10^{18}$–$1 \times 10^{21}$ Pa s |
| | Matrix viscosity ($\mu_m$) | $1 \times 10^{19}$ Pa s |
| Bulk strain rate | | $2 \times 10^{-14}$ s$^{-1}$ |

Twelve folds have been developed (Fig. 1b), which differ in the viscosity contrast between layer and matrix ($m = 10$, 25 and 100) and anisotropy ($a = 1$, 5, 10 and 50). For $m \neq 100$ or anisotropic behaviour, the initial wavelength/thickness of the perturbation is larger than the one that develops at maximum growth rate. However, for $m = 10$ and $m = 25$, the growth rate of the selected perturbation is only 0.65 and 0.85 times lower than the dominant wavelength/thickness.

In all the folds, the geometrical data, and principal values and directions of strain in every element were obtained at 5% shortening intervals, thus providing complete knowledge of the evolution of the folding. The models were run to bulk shortening values of up to 40–65%. However, when $\mu_s$ is similar to or lower than $\mu_m$ there are stability problems in the models and it is not possible to reach those bulk shortening values. For these models, there was a strong tendency to generate new instabilities with shorter wavelengths than the initially prescribed perturbation; these short wavelengths are related to the smallest length defined by the finite-difference mesh. Comparable observations were previously reported by Mühlhaus et al. (2002) and were interpreted as an effect of ignoring the couple stress across the layer in anisotropic materials.

The advantage of performing kinematical analyses on numerical folds mainly lies in the precise information available on geometrical and strain properties at every point of the folded layer, which makes it possible to make a study of the kinematical behaviour of the folded layers. Nevertheless, we must be very careful when generalizing the results since the models have been developed in accordance with specific properties: isolated layer welded to the incompetent matrix, with a specific initial perturbation and with certain geometric and mechanical characteristics.

## 3. Kinematical analysis method

We used the *FoldModeler* program (Bobillo-Ares et al., 2004) written in the MATHEMATICA™ environment to perform the kinematical analysis of the folds. In this program the layer is discretized in a grid of points grouped in quadrilaterals, where every point is perfectly defined in a coordinate system. The positions of the points of this initial layer are transformed in accordance with the geometric laws of the different mechanisms. The program is able to apply the transformations arising from tangential longitudinal strain (TLS), flexural flow (FF) and irrotational homogeneous deformation (HD). The user decides the sequence in which the mechanisms operate. A strain pattern sequence is built up in steps, representing operation of one mechanism. The analysis of the final configuration enables the data relating to the final geometry of the layer (normalized amplitude, shape of the folded surface and layer, etc.) to be collected, and by comparing the position of each initial quadrilateral with its deformed final shape,

Cauchy's tensor is obtained, from which the principal strain values and directions are calculated at each point of the folded layer.

Determining, using *FoldModeler*, the sequences of folding mechanisms that are responsible for strain accommodation, requires all or some of the following information about the analysed fold (Fig. 2):

1. The initial geometry of the layer, which consists of the thickness/length relationship of the layer, the normalized amplitude ($h = y/x$) of the initial irregularity and the morphology of the guide line (GL). The GL is a line located within the layer, initially parallel to its boundaries and represents the line to which the point transformations during the folding process are referred. In TLS, the GL is the neutral line. The GL's morphology is determined using the method described in Aller et al. (2004).
2. The maximum dip in the final configuration of the GL and final relationship $t_0/y_{oa}$ (thickness in the hinge zone divided by the amplitude of the outer arc).
3. The final normalized amplitude ($h$) of the layer and final shape of the GL.
4. The bulk shortening produced by the folding.
5. The relationships $\phi-\alpha$ (variation of $\lambda_1$ direction with the dip $\alpha$) and $R-\alpha$ (variation of the relationship $\sqrt{\lambda_1/\lambda_2}$ with $\alpha$).
6. Ramsay's classification of the folded layer to determine variations in layer thickness (Ramsay, 1967, pp. 359–372).

To analyse the strain patterns that have operated in a fold, we use *FoldModeler* to construct an initial grid that has the same characteristics as the modelled fold. Subsequently, by a trial-and-error process, we run the necessary number of different sequences of strain patterns until the best fit for the final data is obtained. Therefore, using *FoldModeler* to fit a fold involves constructing a theoretical fold with this program that is similar, in all respects, to the fold under analysis.

Throughout this paper we will compare the relative importance of the different strain patterns in the strain accommodation with the folding development. To quantify the intensities of the mechanisms, for TLS and FF we considered the change of $h$ that the layer undergoes as a result of the operation of these mechanisms. That is to say, for a fold that accommodates the strain by TLS (producing a variation of $h = 0.7$) at an early stage and is later deformed by FF (producing a variation of $h = 0.1$), the intensities of TLS and FF will be 0.7 and 0.1 respectively. Therefore, TLS would be predominant and the final deformation pattern in the fold will be more similar to the pure TLS than to the pure FF. In the case of HD, we measured its intensity as $|e_2|$, that is to say, the absolute value of the longitudinal stretch in the $\sqrt{\lambda_2}$ direction.

In *FoldModeler*, each folding step only involves one pure mechanism, and the sum of all of these will form the sequence of strain patterns of the fold. This means that simultaneity cannot be performed. Nevertheless, it is possible to simulate this effect by considering alternating steps of small magnitude. For instance, in the above example, simultaneity can be simulated by running the TLS + FF sequence ten times given the following amounts of TLS and FF for each step: $\Delta h_{TLS} = 0.07$ and $\Delta h_{FF} = 0.01$.

## 4. Results of the fits

To obtain fits to the FLAC folds, we measured all the aforementioned geometrical data, plotting the relationships $\phi-\alpha$ and $R-\alpha$ in the outer and inner arc of the folded layer, and positioning the initial GL in the middle of the layer. We performed two types of fits, one in which only the final stage of folding (type 1) was considered, and another in which the

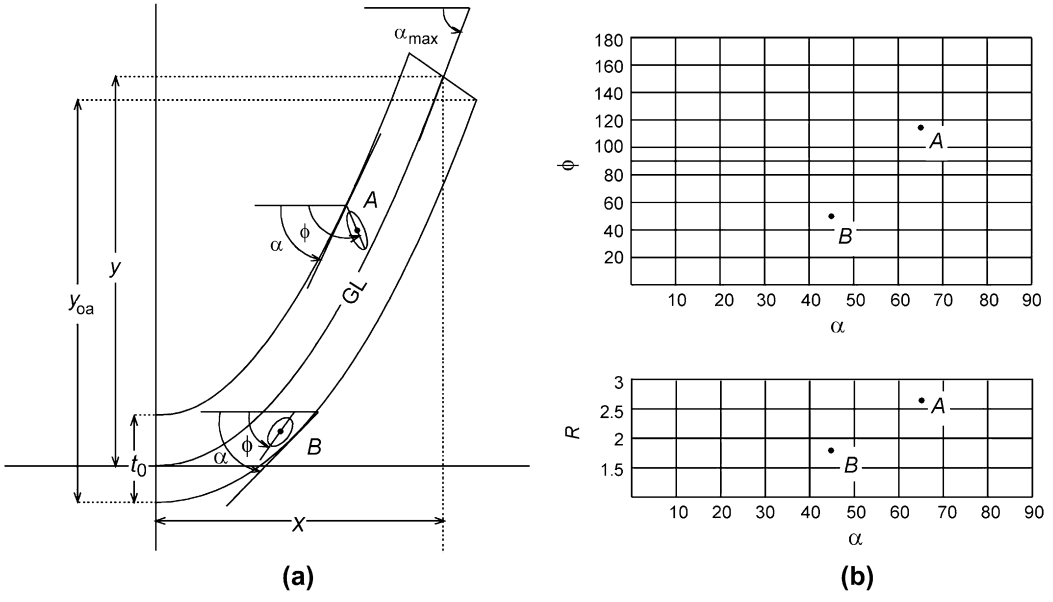


Fig. 2. (a) Definition of geometrical parameters measured in a fold. (b) Diagrams to show the relationships $\phi-\alpha$ and $R-\alpha$. Examples of $A$ and $B$ points for the fold represented in (a).

intermediate stages were taken into account (type 2). These two types of fits were used to check whether the results obtained by only analysing the final stage (as usually occurs in nature) are different from those obtained considering the intermediate stages.

For all the modelled folds, the best-fit sequence of folding mechanisms is always the same. The sequence only differs in the relative intensities of the mechanisms, which will depend on the mechanical properties of the folded layer and on the bulk shortening undergone (Toimil, 2005). However, we should point out that we were not able to study the influence of late-stage flattening (very common in nature), since numerical model folds could not be developed up to the stage where this mechanism takes place. Therefore all the irrotational homogeneous deformation necessary to fit the models will always be associated with the first folding stages as initial layer shortening (ILSH).

Because there is exact knowledge of the input parameters for *FoldModeler* in the FLAC folds, the variability of the fits that can be obtained in a fold is very small. We observed that the folds need a specific intensity of every strain pattern, and the different mechanisms that form the sequence have to be combined in accordance with a very definite order (Toimil, 2005).

### 4.1. Results obtained with type 1 fits

We performed many different fits by varying the amount of intensity of each strain pattern and the order of the strain patterns in the sequence. The variation of the strain pattern intensities is very small (Fig. 3), reaching a maximum value of $\Delta h = 0.05$ for TLS and FF, and $\Delta|e_2| = 0.01$ for ILSH. All the folds need to be fitted with the same sequence that consists of an ILSH step followed by TLS and subsequently FF. ILSH can operate simultaneously with TLS, and FF takes place at the end of the folding process. If this were not so, and TLS was applied after FF, the strain in the inner arc would increase, producing anomalies in the shape of the layer (see i.e. Bobillo-Ares et al., 2000, Fig. 5) and in the $\phi-\alpha$ and $R-\alpha$ relationships, making good fits impossible. This is because TLS, in this case, would be operating on an already amplified fold with high curvature which would cause an increase in the intensity of the strain by TLS.

Regarding the relationship between the mechanisms and the mechanical properties (Fig. 3), the intensity of ILSH decreases as the viscosity contrast increases (something already stated by other authors, i.e.: Ramberg, 1964; Hudleston, 1973; Hudleston and Stephansson, 1973). Increase in anisotropy also produces the same decrease, although its effect is less marked. This could be because part of the deformation that should be accommodated by ILSH, is accommodated by FF with the increase in anisotropy, since the ease of layer parallel shear increases.

The relative importance of TLS with respect to other strain patterns increases when the viscosity contrast increases. FF intensity also increases with viscosity contrast but to a lesser extent than TLS. The role of FF as the dominant strain pattern is related to materials with high anisotropies, although this mechanism even appears, at small intensities, in isotropic materials. In general, for folds developed in

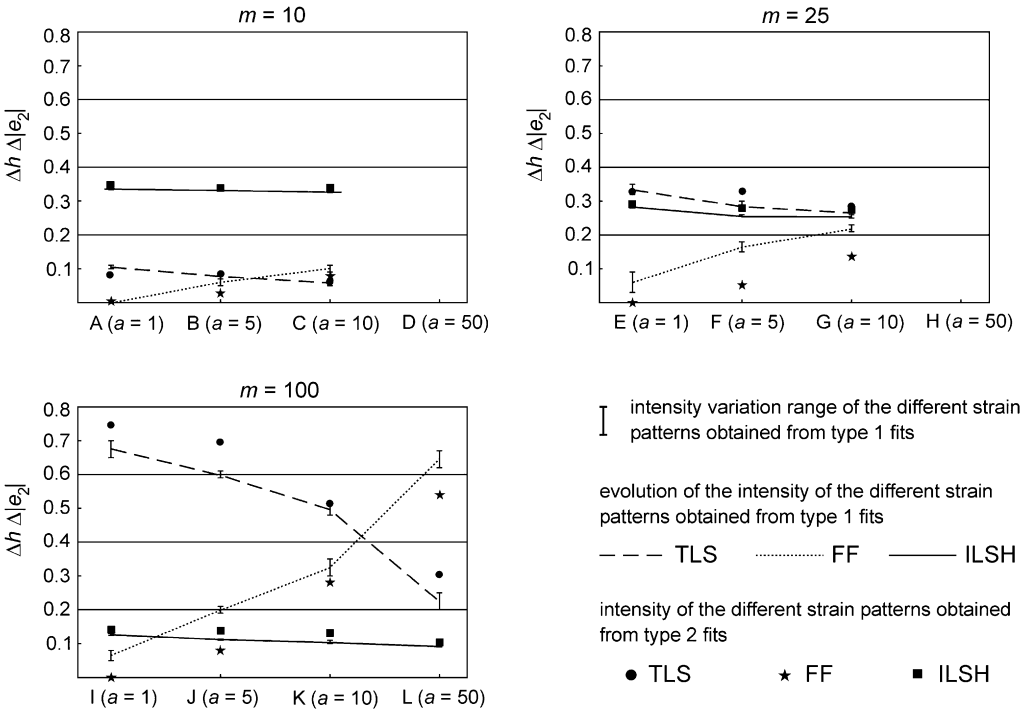


Fig. 3. Comparison between the results of type 1 fits with type 2 fits for all the folds analysed at the 35% shortening stage. Each diagram represents folds with the same viscosity contrast. Folds with different anisotropy are located in the X-axis. The Y-axis represents the intensity of the different strain patterns, with the same scale for TLS and FF (intensities measured as $\Delta h$) and for ILSH (intensity measured as $\Delta|e_2|$).

competent layers with low anisotropy, TLS dominates over FF. Therefore, an increase in anisotropy and viscosity contrast favours the predominance of TLS and FF over ILSH, which leads to a larger amplitude ($h$) for the same amount of bulk shortening.

### 4.2. Results obtained with type 2 fits

Type 2 fits are especially useful for elucidating the evolution of the different strain patterns throughout the folding, since they consider the intermediate stages. Because of this, in addition to the aforementioned relationships, new ones appear (Fig. 4). During the more initial stages, the contribution made by ILSH is similar regardless of viscosity contrast. The intensity of this mechanism remains more or less constant during the folding process with low viscosity contrast ($m = 10$), while it tends to decrease or even disappear in folds with higher viscosity contrasts ($m = 25$ and $m = 100$). There is a marked decrease in ILSH in folds with $m = 25$ for bulk shortening values between 30% and 40%, and in layers with $m = 100$ marked decreases occur for 10–15% of bulk shortening. Hudleston (1973), from experiments carried out in linear viscous materials, and Hudleston and Stephansson (1973), applying the finite element method to Newtonian substances, state that ILSH almost completely disappears once the limb of the fold reaches a dip of 10–25°. Using the results of the *FoldModeler* fits we built Fig. 5, which represents the amount of incremental strain at certain limb dips (the limb dip increases as does the bulk shortening). We observed that there is not a strong decrease in ILSH in the range of dips given by these authors, and it seems that the decrease in ILSH as the fold amplifies is more gradual and disappears at the highest dips. The disappearance angle is related to the viscosity contrast between the layer and the medium, in such a way that as the viscosity contrast increases, the angle becomes smaller. However, there does not seem to be any influence of the layer anisotropy.

In intermediate stages of folding evolution, TLS and FF are the dominant mechanisms (Fig. 4). In folds developed in anisotropic layers, as folding progresses, there is a gradual decrease in the amount of TLS and an increase in FF, which is probably due to the geometrical incompatibilities concerning TLS. This corroborates with what we obtained with type 1 fits where to achieve good fits in a certain fold, FF had to operate after TLS. In theoretically isotropic folds $a = 1$, we observed that FF is not necessary for this type of fit. Instead, TLS intensity increases as the fold develops.

The cumulative intensities of each mechanism in type 2 fits, that is to say, the sum of the intensities of one mechanism throughout the previous stages until reaching a certain stage, are very similar to those obtained with type 1 fits (Fig. 3). Nevertheless, there are small differences that especially affect the relative contributions of TLS and FF; in this way, it seems that if we do not consider intermediate stages (type 1), more FF and less TLS is necessary than if we take all the stages into account (type 2). This has certain implications, for instance, if type 1 fits are made, some FF may be necessary in isotropic materials. However, since the sequence obtained with type 2 fits is similar to that achieved with type 1 fits, both in the order

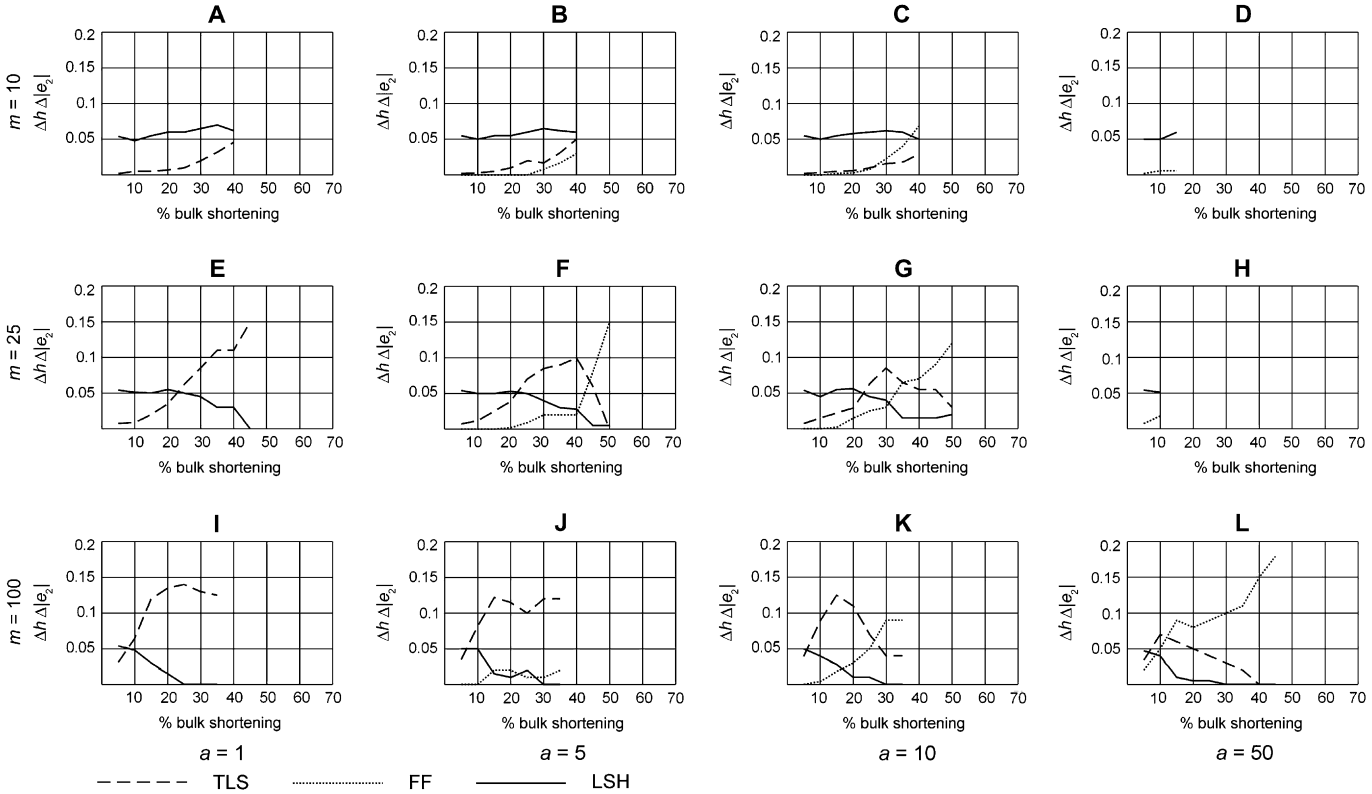


Fig. 4. Intensity variation of the different strain patterns ($\Delta h$ for TLS and FF, and $\Delta|e_2|$ for LSH) obtained from type 2 fits at 5%-shortening intervals.

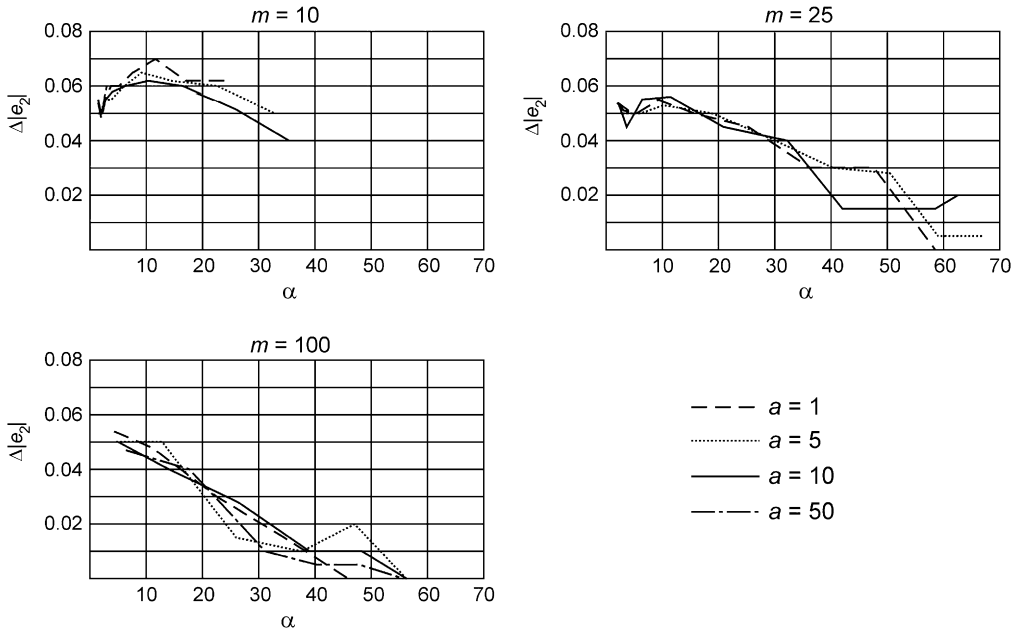


Fig. 5. Variation of the layer shortening intensity ($\Delta|e_2|$) with layer dip ($\alpha$).

of the different mechanisms and in their intensities, we can state that in folds where there is a lack of information about intermediate stages, the analysis of the final stage is sufficient to provide representative kinematical information about the fold.

In type 2 fits, the variation of the strain pattern intensities almost disappears (they are below the fourth decimal place for $\Delta h$ and $\Delta|e_2|$), since any sequence that fits a fold in a certain stage has to be compatible with the subsequent stages. This fact strongly reduces the intensity variation; therefore we have obtained only one sequence that fits each fold.

## 5. Problems with the fits

Type 1 and type 2 fits give good fits of the geometrical parameters of shape, Ramsay's classification, $t_0/y_{oa}$, bulk shortening, as well as $\phi-\alpha$ data in the inner and outer arc. However, certain problems arise (Toimil, 2005):

1. There are no good fits of the $R-\alpha$ in the inner arc, since *FoldModeler* delivers much higher strains in this zone (Fig. 6).

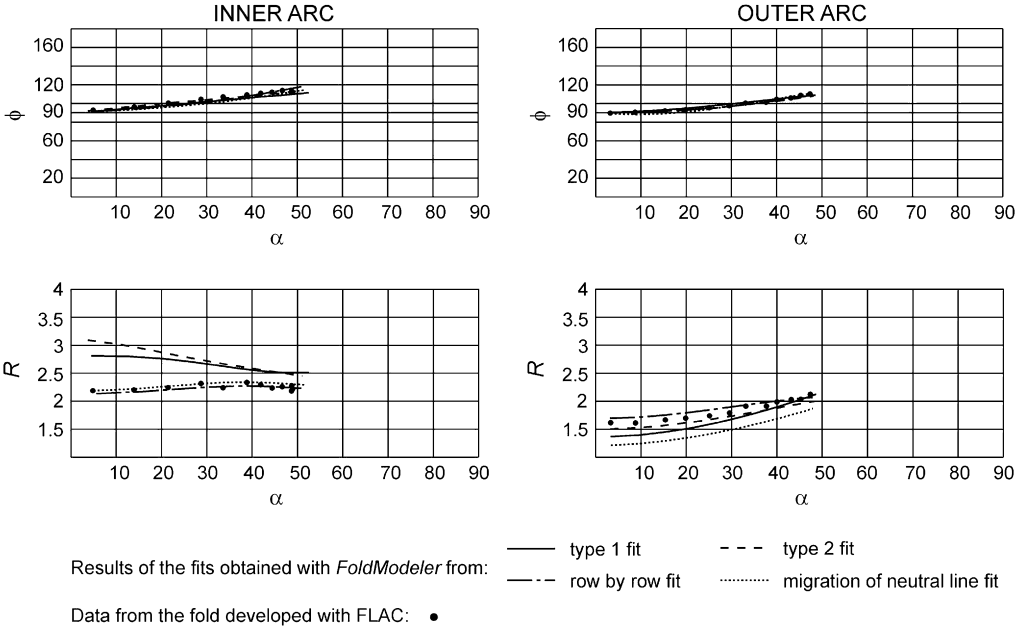


Fig. 6. Fits of the $\phi-\alpha$ and $R-\alpha$ data in the outer and inner arc of the fold G at 40% shortening. Curves obtained from type 1 fits, type 2 fits, migration of neutral line fits and row-by-row fits.

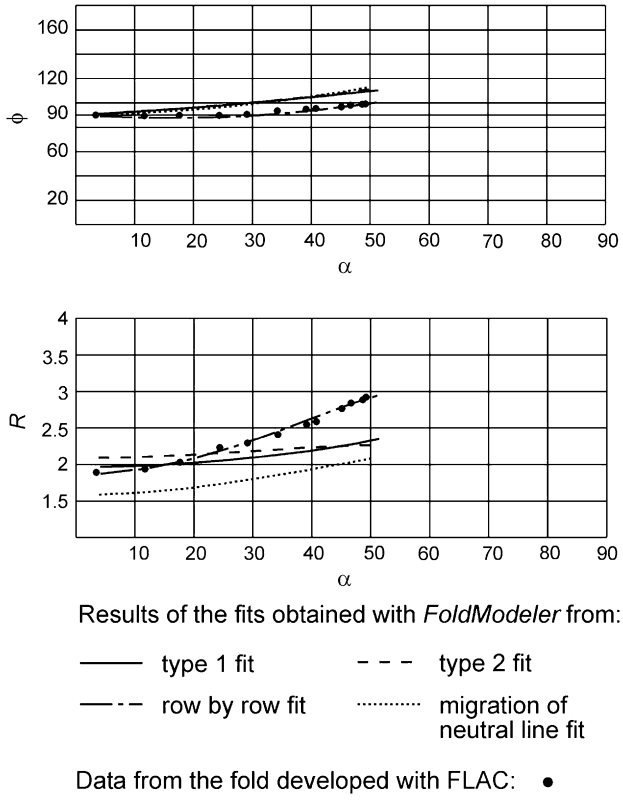


Fig. 7. Fits of the $\phi-\alpha$ and $R-\alpha$ data in a central row of the fold G at 40% shortening. Curves obtained from type 1 fits, type 2 fits, migration of neutral line fits and row by row fits.

2. The fit of $\phi-\alpha$ and $R-\alpha$ relationships worsens towards the centre of the folded layer, that is to say, the misfit of the data becomes larger as we move away from the layer boundaries (Fig. 7).
3. There are differences in the morphology of the layer at the inflection point between the shape obtained with *FoldModeler* and the shape of the analysed fold. While the fit with *FoldModeler* produces a straight morphology (Fig. 8), that of the FLAC fold is sigmoidal. This kind of sigmoidal morphology was achieved by Ramberg (1961) and Hudleston et al. (1996). The mechanical reason for this morphology is that the layer-parallel shear stress is higher in the middle of the layer than at the edges. In any case, there is a need to find the strain distribution that fits the sigmoidal morphology.

The lack of fit could be because the mechanisms considered in the *FoldModeler* program are not the only ones able to accommodate strain in folded layers. In this regard, we tried to solve the described problems by considering the influence of other mechanisms or by modifying those already considered (TLS, FF and ILSH).

### 5.1. Neutral line migration

We considered the effect of migration of the neutral line in order to try to solve the problem related to the high strain in the inner arc zone. *FoldModeler* does not permit the simulation of a progressive migration, since the location of the neutral line has to be linked to the same particles during the folding. Therefore, to model this effect we placed the GL in a position closer to the inner than the outer arc instead of in the centre of the layer as we did for the type 1 and 2 fits. We are aware that this is not a "real" neutral line migration, but this kind of simulation gives results similar to what is expected with progressive neutral line migration.

Although in principle this mechanism can offer a solution to the problem of the high strain in that zone, its operation creates other problems in the outer arc, since the increase in the distance between the neutral line and the outer boundary causes an increase in the extensional stretching in this area (Ramsay and Huber, 1987, fig. 21.21). Fig. 6 shows this effect: the fit of the $R-\alpha$ curve in the inner arc improves whereas in the outer arc it worsens. On the other hand, the influence on the $\phi-\alpha$ curves is small. Apart from this, neutral line migration does not solve the problems related to the worsening of the $\phi-\alpha$ and $R-\alpha$ towards the centre of the fold (Fig. 7) or to the morphology of the layer at the inflection point zone (Fig. 8).

### 5.2. Heterogeneous area change

Ramsay (1967, pp. 401–402) states that the problem of the high strain in the inner arc in folds formed by TLS can be solved if there is a decrease in area in this zone. Hudleston

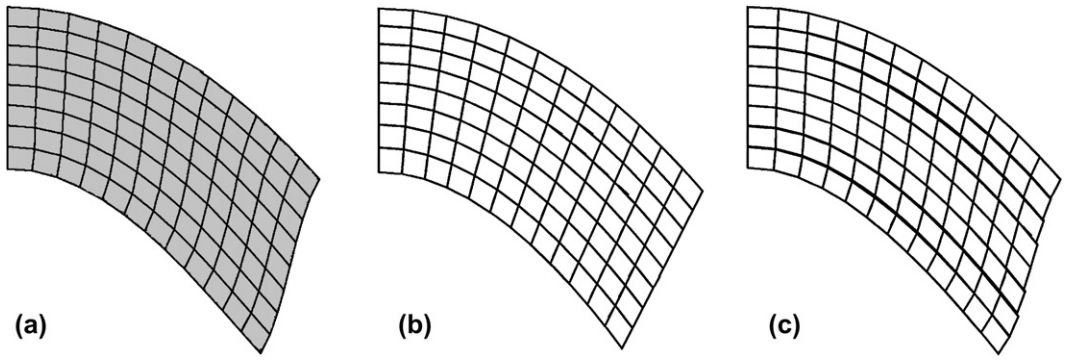


Fig. 8. (a) Fold G of FLAC at 40% shortening. (b) Fold obtained from type 1, type 2 and migration of neutral line fits. (c) Fold obtained from row by row fits.

and Holst (1984) propose a way of strain accommodation that also implies area change, which they refer to as ''inner arc collapse''. Heterogeneous area changes cannot be modelled with *FoldModeler*. Nevertheless, we estimated how much decrease in area would be necessary for the *R* values given by *FoldModeler* to be similar to those of the folds analysed. To do this, we assumed that, in the inner arc, the shortening in $\lambda_2$ direction obtained theoretically with *FoldModeler* is the same as that produced in the FLAC fold. Therefore, as we know $\sqrt{\lambda_2}$ and the *R* value that we want to fit, it is possible to calculate the area variation. We performed the study for 35% of the bulk shortening stage in the inner arc of the hinge zone in all the folds (Table 2). The decreases in area are much larger than 1% (the value of decrease in area in the FLAC folds), except in the folds with less viscosity contrast. Therefore, decrease in area associated with the FLAC models does not provide the solution to the problem. Furthermore, it does not solve the fits in the central rows of the layer or the problem related to the morphology of the layer at the inflection point.

Table 2
Percentage decrease in area necessary to fit *FoldModeler R* values with FLAC *R* values

| | | | | |
|---|---|---|---|---|
| $m = 10$ | 0–1.79 | 1.49–2.42 | 0–1.45 | – |
| $m = 25$ | 6.89–17.16 | 7.97–20.55 | 11.71–20.06 | – |
| $m = 100$ | 4.58–25.25 | 13.30–36.98 | 13.36–19.04 | 10.97–17.02 |
| | $a = 1$ | $a = 5$ | $a = 10$ | $a = 50$ |

Inner arcs at hinge zones of folds at 35% shortening have been considered.

### 5.3. Row-by-row fits

Row-by-row fits consist of fitting every row of quadrilaterals of the folded layer independently. In principle this leads to an incompatibility problem (Fig. 8c), since when the different rows are joined to build the layer, discontinuities appear in lines that should be continuous. However, these discontinuities are not very large. Besides, we should consider that the fits represent approximations of the kinematical behaviour of the folds, which means that, although they must be taken into consideration, they can be assumed to carry out the analysis of the folds to look for better fits of all geometrical parameters. The use of the row-by-row fits solves the three main problems described earlier: the high value of the deformation in the inner arc of the folded layer (Fig. 6), the lack of fit of the central rows of the fold (Fig. 7), and the strain distribution that justifies the morphology at the inflection point zone (Fig. 8).

## 6. Implications of row-by-row fits

The results obtained with the row-by-row fits show a series of characteristics that affect the traditional concept of TLS and the distribution of the different strain patterns (ILSH and FF) across the layer (Toimil, 2005). These characteristics appear in all the folds, regardless of the value of the anisotropy or viscosity contrast.

### 6.1. Initial shortening of the layer

The ILSH of the layer is not homogeneous, but there is a small variation of shortening across the layer (Fig. 9), tending to increase in zones close to the inner arc and to decrease near the outer arc, and remaining practically constant in the central parts.

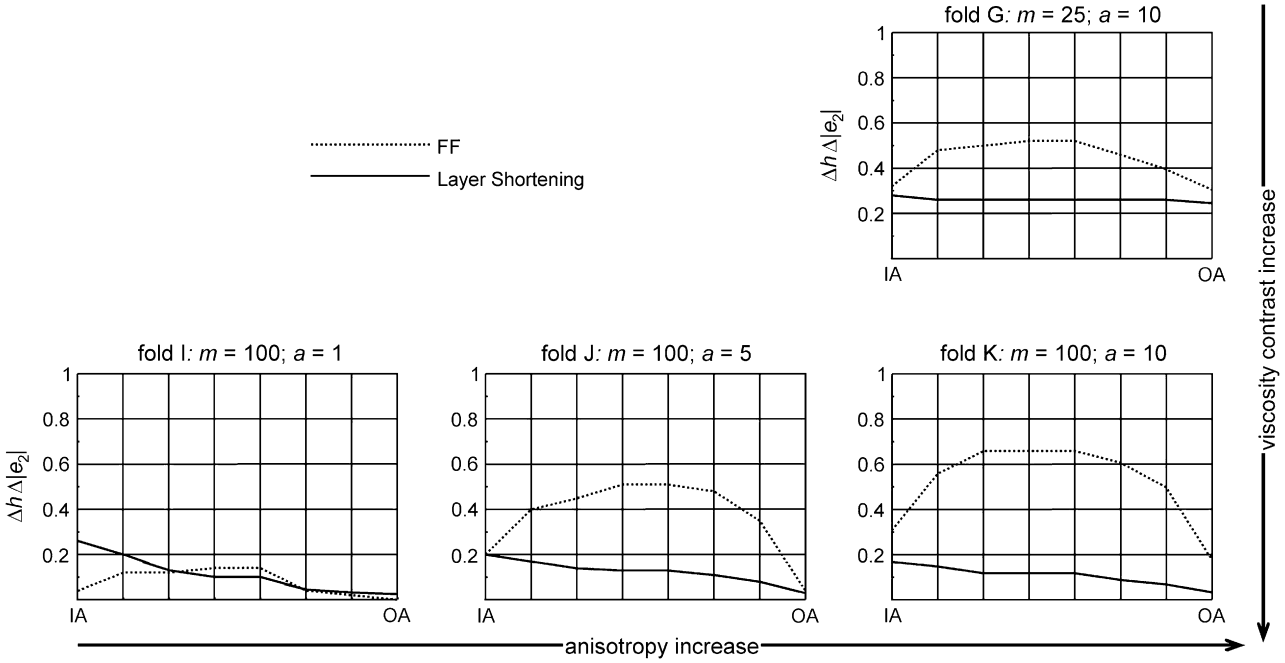


Fig. 9. Intensity variation of FF and LSH across the layer, from the inner arc (IA) to the outer arc (OA). Results obtained from row-by-row fits for different folds at 40% shortening.

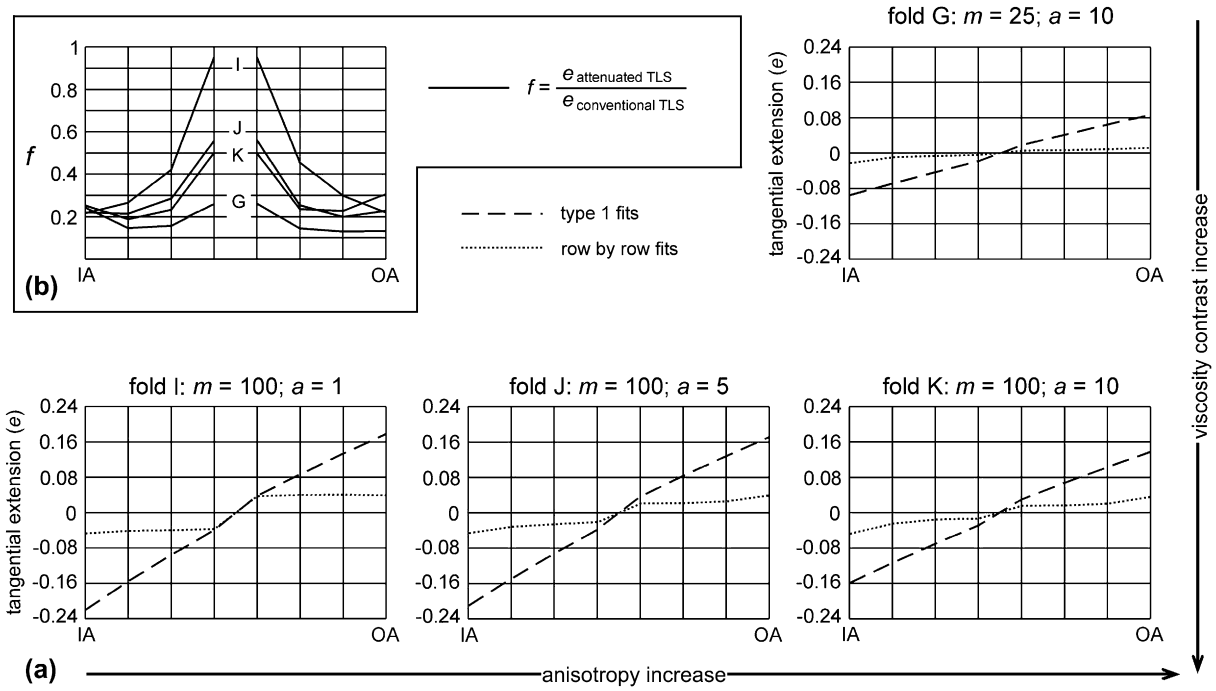


Fig. 10. (a) Comparison between tangential extension across the layer, from the inner (IA) to the outer arc (OA), in conventional TLS (type 1 fits) and attenuated TLS (row by row fits). Results obtained from different folds at 40% shortening. Y-axis represents stretching ($e > 0$) and shortening ($e < 0$). (b) Relationship ($f$) between conventional TLS extension and attenuated TLS extension.

### 6.2. Tangential longitudinal strain

The amount of TLS that operates is lower that when the entire layer is analysed as a whole, and represents, therefore, an ''attenuated TLS'' (TLS*). In Fig. 10a, we compare the tangential extension produced by TLS across the layer for type 1 fits (conventional TLS) with row-by-row fits (TLS*) in the folds G, I, J and K for the 40% shortening stage. We observed that the row-by-row fit provides a smoother variation across the layer.

The deformation intensity by TLS from a flat layer is given, approximately, by the following expression (see e.g. Ramsay, 1967, eq. 7.19):

$$e = \frac{t'}{r} \tag{2}$$

where $e$ represents the tangential extension, $t'$ the distance to the neutral line and $r$ curvature radius. Taking this into account, so that eq. (2) gives the intensity produced by TLS*, the right hand side of the equation should be multiplied by a factor $f$ less than one. On studying this factor, we observed that it is not constant (Fig. 10b) and varies across the layer showing a dependence on the viscosity contrast ($m$) and anisotropy ($a$). Thus, eq. (2) for TLS* could be represented by:

$$e = \frac{f(t', m, a)}{r} \tag{3}$$

being $f(t',m,a)$ a factor that is a function of $t'$, $m$ and $a$ and fulfilling that $0 \geq f(t',m,a) \geq t'$. In the closest zones to the GL, in this case towards the central parts of the layer, the factor $f$ is larger, which means that in these zones TLS* is more similar

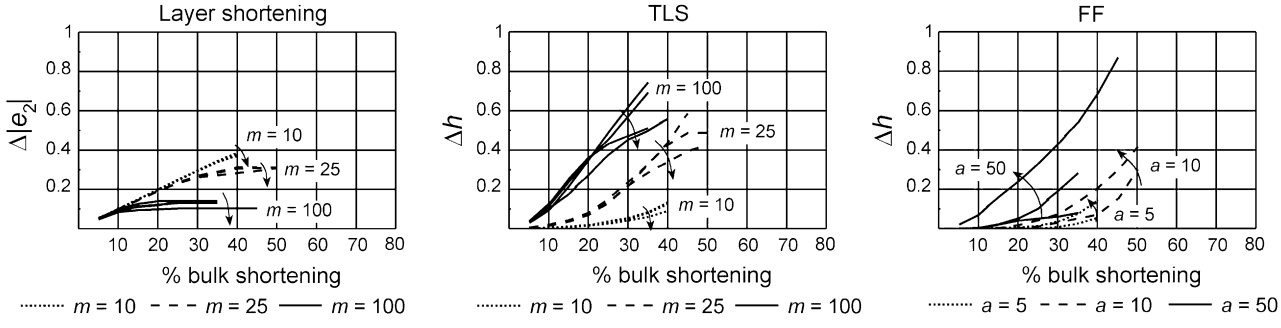


Fig. 11. Relationship between the intensities of the different strain patterns and mechanical properties: viscosity contrast ($m$) and anisotropy ($a$). Each curve in the diagrams represents the cumulate intensity of one strain pattern. Curves are grouped according to viscosity contrast (in TLS and LSH) and anisotropy (in FF). In every group, arrows indicate increase in anisotropy (in TLS and LSH) and increase in viscosity contrast (in FF).

to conventional TLS. Likewise, if the viscosity contrast remains constant, $f$ increases when the anisotropy decreases (compare fold J, $a = 5$, with fold K, $a = 10$). If the viscosity contrast is modified, keeping the anisotropy constant, $f$ will increase as $m$ increases (compare fold G, $m = 25$, with fold K, $m = 100$).

### 6.3. Flexural flow

In the classical definition of FF (Ramsay, 1967, pp. 391–397), the angle of the layer dip was the only variable that influenced its intensity, fulfilling $\alpha \approx \gamma$, $\alpha$ being the angle of dip in radians at every point of the fold and $\gamma$ the shear strain at this point. However, from the row-by-row fits, we observed that the largest intensity of FF is located in the centre of the layer and decreases towards the boundaries (Fig. 9). Besides, the FF intensity increases as the anisotropy increases and to a lesser extent as the viscosity contrast increases. This mechanism even occurs in isotropic material.

The increase in FF intensity towards the centre of the layer can also be seen in the models that Hudleston et al. (1996) developed to analyse the importance of FF in nature. In those models, the strain markers (lines initially perpendicular to the layer boundaries) undergo a distortion that matches the FF pattern, and this is more important in the centre of the layer. Moreover, it can also be seen that as the anisotropy increases the distribution of strain within the layer becomes more similar to FF.

## 7. Viscosity contrast and anisotropy estimation

In geological literature, many methods to estimate the viscosity contrast between the competent layer and the incompetent matrix have been developed. Biot (1961) derived an equation that enables this calculation from the ratio between the dominant wavelength and the thickness of the layer. Sherwin and Chapple (1968) modify Biot's equation to include the influence of the initial layer shortening. Hudleston (1973) applies Sherwin and Chapple's expression to Newtonian viscous models, taking into account Chapple's (1968) wavelength selection theory and that beyond a limb dip of approximately 15° there is no initial layer shortening. Shimamoto and Hara (1976) work out viscosity contrasts in natural folds on the basis of the work done by Hudleston (1973) and on the finite element models that they developed. Lisle et al. (1983) establish a method to estimate the viscosity contrast between pebbles and the matrix in which they are embedded. Treagus (1983, 1988, 1999) estimates the viscosity contrast from the angular relationships of the cleavage refraction in two adjacent layers. Subsequently, Schmalholz and Podladchikov (2001) develop a method to estimate the bulk shortening and the viscosity contrast in viscous and viscoelastic materials by measuring two geometrical parameters in the folds: the thickness/wavelength ratio, and the amplitude/wavelength ratio. In this paper, we propose a new method for estimating viscosity contrast and anisotropy of the folds taking into account their kinematical characteristics. This method does not intend to replace any of those described above, but represents an alternative method, and therefore, another way of deriving some mechanical characteristics of natural folds.

### 7.1. Viscosity contrast estimation using fitting sequences

From the data obtained with the type 2 fits of the FLAC folds, we plotted the cumulative intensities of each mechanism versus bulk shortening (Fig. 11). The cumulative intensity curves display grouping patterns that define certain fields. Thus, in the TLS and ILSH diagram, those curves corresponding to folds with the same viscosity contrast appear together, whereas for FF they are grouped in accordance with anisotropy. Therefore, in general, TLS and ILSH intensities are essentially functions of the viscosity contrast between layer and matrix, whereas FF mainly depends on the anisotropy. Nevertheless, there are several tendencies within each group. Thus, for TLS and ILSH, an increase in anisotropy is represented as a decrease in the slope of the curves, and in FF the increase in the slope of the curves is related to the increase in viscosity contrast.

These fields can be used to estimate the viscosity contrast and anisotropy of a certain fold when we know the cumulative intensities of each mechanism and the bulk shortening undergone, having previously obtained this information by means of kinematical analysis using *FoldModeler*. Nevertheless, there are certain limitations due to that diagram (Fig. 11) being based on the kinematical study of specific numerical models. Therefore, apart from the general restrictions already mentioned for the FLAC folds, several considerations must also be made:

1. The plot has been made from type 2 fits, therefore, strictly, it is only valid for folds for which intermediate stages of folding have been analysed. However, we checked that the data obtained with type 1 fits also provide a good estimate of viscosity contrast. In the case of anisotropy, the results are not so good, generally leading to an overestimation of this mechanical property. This is because FF is used to estimate the anisotropy value, and the intensity of FF reached with type 1 fits is larger than that achieved with type 2 fits.
2. On the other hand, the fields of the plot do not completely cover the diagram, because the models analysed have a restricted range of values of anisotropy and viscosity contrast. Clearly, any fold that has $m$ and $a$ values over 100 and 50 respectively or a large bulk shortening, will lie outside these fields.

### 7.2. Validation of this method and natural example

To validate this method, several examples of folds published by other authors have been analysed. We selected some symmetrical folds developed in competent layers (Dieterich, 1970, fig. 5a, 5b and 6a; Shimamoto and Hara, 1976, fig. 6f; Anthony and Wickham, 1978, fig. 2). The results provide a good estimate of viscosity contrast (Fig. 12), although the data concerning each fold generally lies outside

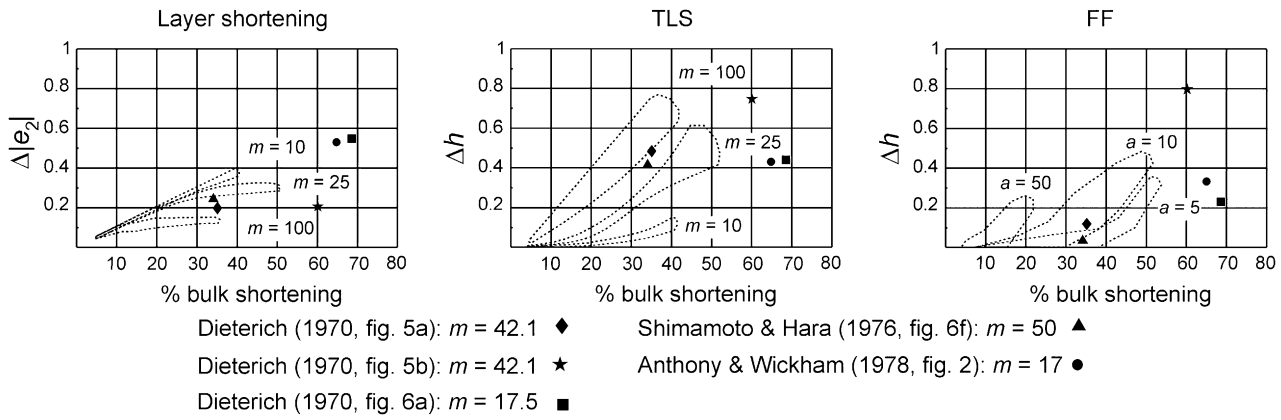


Fig. 12. Plot of the results of type 1 fits performed in finite-element folds (developed by different authors) in the diagrams of Fig. 11 in order to validate the method proposed. The dotted lines defining the fields represent the location of groups of lines in Fig. 11 with the same viscosity contrast ($m$), in case of ILSH and TLS, and anisotropy ($a$), for FF.

the fields defined by this study. These fields must be extrapolated to determine the $m$ values. Regarding the anisotropy, although all the analysed models are isotropic, the diagram provides a certain value of this property. Anisotropy is overestimated because we carried out type 1 fits to analyse these folds, therefore a larger value of FF is obtained which leads to a larger anisotropy value.

From these results, it can be seen that the method could be improved if other models, with different values of viscosity contrast and anisotropy, were to be studied. It would also be interesting to extend the study to other materials with different rheological properties as well as to folds affected by flattening. Thus, general diagrams of mechanisms can be built to estimate viscosity contrast and anisotropy through knowledge of the sequence of strain patterns and the bulk shortening undergone.

We also used *FoldModeler* to analyse a natural fold developed in a sandstone layer from the western part of the Iberian Massif in order to estimate its mechanical properties (Fig. 13). This fold is located in an area of greenschist facies metamorphism affected by a stage of folding with associated cleavage. We gathered all the geometrical data from this fold in order for it to be fitted using *FoldModeler*: normalized amplitude, $t_0/y_{oa}$ parameter, shape of the folded layer, the relationships $\phi-\alpha$ (where strain data is absent, we assume that the intersection of the cleavage plane with the fold profile is parallel to $\lambda_1$) and $R-\alpha$. The strain was calculated using Fry's (1979) method. We performed a large amount of type 1 fits (one of which is shown in Fig. 13) to constrain the intensity values of the different strain patterns, and we have seen that all the sequences show a good fit of all the geometrical features except for the strain in the inner arc. This problem is studied by Toimil and Fernández (in press). The fitting sequences are very similar in terms of both the order of the folding mechanisms and their importance. To estimate the mechanical properties we used the intensities of ILSH, TLS and FF, which have a variation range of 0.18–0.20 (ILSH), 0.32–0.46 (TLS) and 0–0.10 (FF). The estimation of the viscosity contrast using TLS and ILSH gives the same value $m = 25$, and the value of the anisotropy ranged between $a = 0$ and $a = 5$. Considering that the anisotropy value is likely to be overestimated using the results of FF obtained with type 1 fits, we could state that in the layer analysed the anisotropy is virtually nil. We should take into account that the intensity of the strain patterns (especially for ILSH) will depend on the size of the initial irregularity. In this case we considered that the layer is almost horizontal at the beginning of the folding process ($h$ of the initial perturbation equals 0.001).

## 8. Conclusions

Numerical models of folds with different values of viscosity contrast and anisotropy, developed with the FLAC finite differences program, were analysed using the *FoldModeler* program in order to determine the characteristics of the folding mechanisms that account for strain accommodation. The models have specific properties: isolated layer welded to the incompetent matrix, with a fixed initial perturbation and with certain geometric and mechanical characteristics, which can restrict the applicability of the quantitative results.

A significant finding of this study is that the final geometry of the fold provides enough information to decipher how the deformation was accommodated throughout the folding. The sequence of strain patterns is similar in all the folds analysed, differing only in the relative intensities of each mechanism, which is found to depend on the mechanical properties of the folded layer and the bulk shortening. The sequence starts with initial layer shortening (ILSH) followed by tangential longitudinal strain (TLS) and/or flexural flow (FF). The intensity of ILSH decreases as the viscosity contrast increases. An increase in anisotropy produces the same effect, though to a lesser degree. The stage at which ILSH ceases to be significant depends on the viscosity contrast. An increase in viscosity contrast leads to cessation of ILSH at lower limb dip angles. As the fold amplifies, the deformation tends to be accommodated by TLS and/or FF. TLS is the most important strain pattern in competent layers, although as the folding progresses it is gradually replaced by FF due to its geometrical incompatibilities. The relative importance of TLS with respect

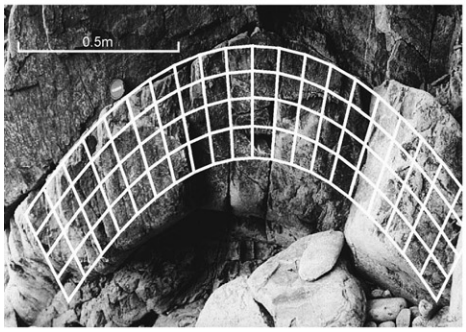


| | natural fold | *FoldModeler* fold |
|---|---|---|
| *h* | 0.790 | 0.773 |
| normalised area* | 1.295 | 1.333 |
| $t_0/y_{0a}$ | 0.750 | 0.788 |
| bulk shortening | - | 42.75% |

* The normalised area is a way of measuring the shape of the folded surfaces (Aller et al. 2004)

type 1 fit
real data
mechanical prop. estimation

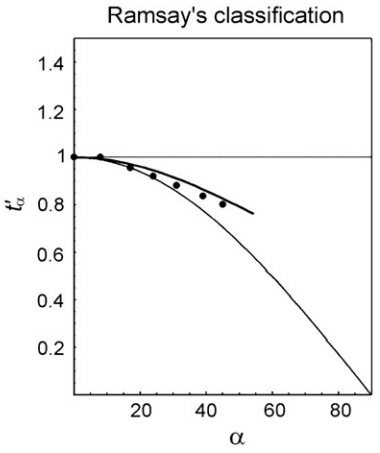


(a)

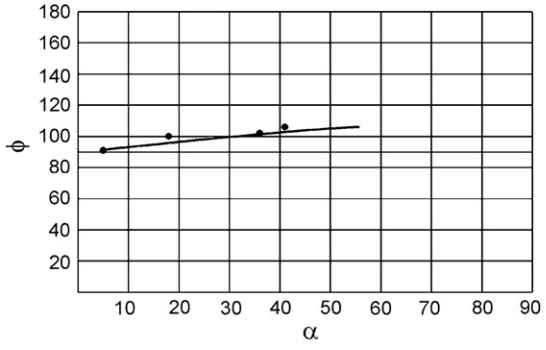


Inner arc

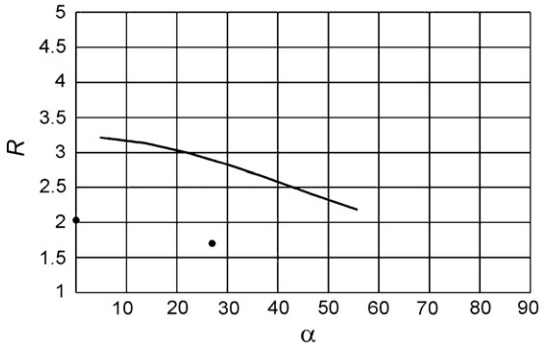


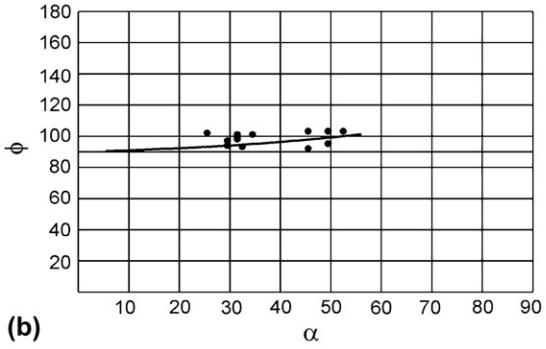


outer arc

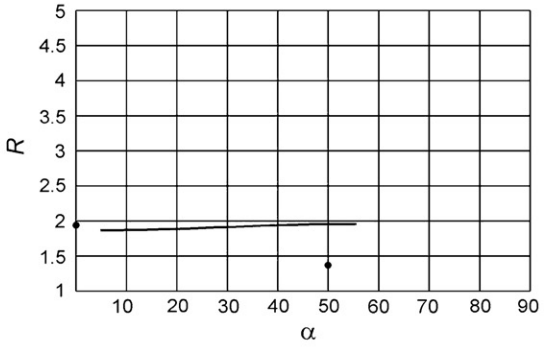


(b)

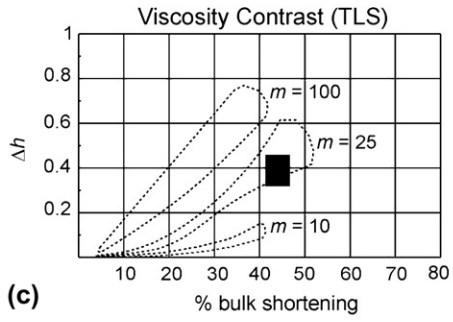


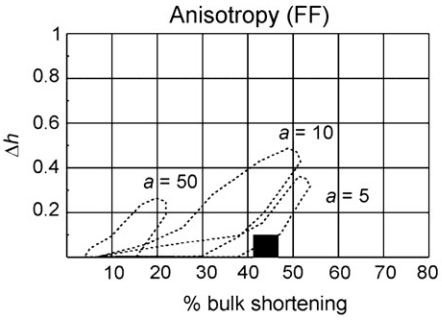


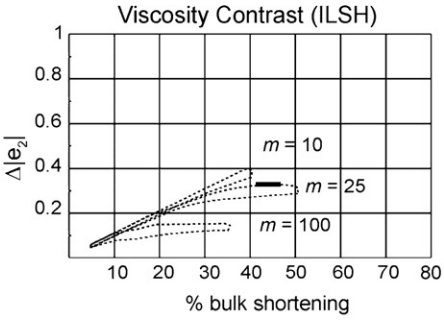


(c)

Fig. 13. Fit of a natural fold and estimation of its mechanical properties. The sequence of strain patterns in this example is formed by ILSH simultaneous with TLS, subsequently TLS and finally FL, and their intensities are: ILSH = 0.19, TLS = 0.46 and FL = 0.2. (a) Theoretical fold obtained using *FoldModeler* (shown in white on the picture of the fold), Ramsay's classification and fit of some geometric properties. (b) $\phi-\alpha$ and $R-\alpha$ diagrams. (c) Estimation of the mechanical properties. The dotted lines defining the fields represent the same as in Fig. 12.

to other strain patterns increases as the viscosity contrast increases. In the case of FF, the larger the anisotropy is, the more intense this strain pattern is. FF intensity also increases as the viscosity contrast increases, but to a lesser extent than TLS. FF even occurs in small quantities in theoretically isotropic materials, and represents the most important mechanism when the anisotropy is very high. Therefore, in general, for folds developed in competent layers with low anisotropies, TLS dominates over FF.

The fit of the folds presents problems regarding strain values in the inner arc and the geometry of the layer. These problems can be solved by performing row-by-row fits. The results of these fits show that ILSH is greater in the inner arc and slightly decreases towards the outer arc, whereas FF reaches a maximum in the central parts of the layer and decreases towards the boundaries. Regarding the TLS, instead of the conventional TLS there is an ''attenuated'' TLS characterized by a much less intense deformation across the layer than for conventional TLS.

The dependences of the intensities of the different mechanisms on the mechanical properties of the layer were used to construct a diagram in which viscosity contrast and anisotropy can be estimated when we know the intensities of ILSH, TLS and FF in the fitting sequence.

## Acknowledgements

The present paper has been supported by the Spanish CGL2005-02233-BTE and CGL2004-03657 projects funded by the Ministerio de Educación y Cultura. We are grateful to the Oviedo Folding Analysis Group and Richard J. Lisle for many valuable suggestions. We would like to thank P. Hudleston, N. Mancktelow and B. Holdsworth for their detailed review of the manuscript, which has notably improved the paper.

## References

Aller, J., Bastida, F., Toimil, N.C., Bobillo-Ares, N.C., 2004. The use of conic sections for the geometrical analysis of folded surface profiles. Tectonophysics 397, 239–254.

Anthony, M., Wickham, J., 1978. Finite-element simulation asymmetric folding. Tectonophysics 47, 1–14.

Bastida, F., Bobillo-Ares, N.C., Aller, J., Toimil, N.C., 2003. Analysis of folding by superposition of strain patterns. Journal of Structural Geology 25, 1121–1139.

Billings, M.P., 1954. Structural Geology, second ed. Prentice Hall, New Jersey.

Biot, M.A., 1961. Theory of folding of stratified viscoelastic media and its implication in tectonics and orogenesis. Geological Society of American Bulletin 72, 1595–1620.

Bobillo-Ares, N.C., Bastida, F., Aller, J., 2000. On tangential longitudinal strain folding. Tectonophysics 319, 53–68.

Bobillo-Ares, N.C., Toimil, N.C., Aller, J., Bastida, F., 2004. 'FoldModeler': a tool for the geometrical and kinematical analysis of folds. Computers and Geosciences 30, 147–159.

Carey, S.W., 1962. Folding. Journal of the Alberta Society of Petroleum Geologists 10, 95–144.

Chapple, W.M., 1968. A mathematical theory of finite-amplitude rock-folding. Geological Society of American Bulletin 79, 47–68.

de Sitter, L.U., 1964. Structural Geology, Second ed. McGraw-Hill, New York.

Dieterich, J.H., 1970. Computer experiments on mechanics of finite-amplitude folds. Canadian Journal of Earth Sciences 7, 467–476.

Donath, F.A., 1962. Role of layering in geologic deformation. Transactions of the New York Academy of Science Series 24, 236–249.

Donath, F.A., Parker, R.B., 1964. Folds and folding. Geological Society of American Bulletin 75, 45–62.

Fry, N., 1979. Random point distributions and strain measurement in rocks. Tectonophysics 60, 89–105.

Gairola, V.K., 1978. Strain distribution across an experimental single-layer fold. Tectonophysics 44, 27–40.

Hobbs, B.E., Mühlhaus, H.B., Ord, A., 1990. Instability, softening and localisation of deformation. In: Knipe, R.J., Rutter, E.H. (Eds.), Deformation Mechanisms. Rheology and Tectonics. Geological Society, London, Special Publications, vol. 54, pp. 143–165.

Hudleston, P.J., 1973. An analysis of ''single-layer'' folds developed experimentally in viscous media. Tectonophysics 16, 189–214.

Hudleston, P.J., Holst, T.B., 1984. Strain analysis and fold shape in a limestone layer and implications for layer rheology. Tectonophysics 106, 321–347.

Hudleston, P.J., Lan, L., 1993. Information from fold shapes. Journal of Structural Geology 15, 253–264.

Hudleston, P.J., Stephansson, O., 1973. Layer shortening and fold-shape development in the buckling of single layers. Tectonophysics 17, 299–321.

Hudleston, P.J., Tabor, S.H., Lan, L., 1988. Strain and fabric development in a buckled calcite vein. Bulletin of the Geological Institutions of the University of Uppsala. N.S 14, 79–94.

Hudleston, P.J., Treagus, S.H., Lan, L., 1996. Flexural flow folding: does it occur in nature? Geology 4, 203–206.

Itasca Consulting Group Inc, 1998. FLAC: Fast Lagrangian Analysis of Continua, Optional Features, version 3.4. Itasca Consulting Group Inc, Minneapolis.

Johnson, A.M., Fletcher, R.C., 1994. Folding of Viscous Layers. Columbia University Press, New York, 461 pp.

Kuenen, P.H., de Sitter, L.U., 1938. Experimental investigation into the mechanisms of folding. Leidsche Geologische Mededeelingen 60, 217–240.

Lan, L., Hudleston, P.J., 1995. The effects of rheology on the strain distribution in single layer buckle folds. Journal of Structural Geology 17, 727–738.

Mancktelow, N.S., 1999. Finite-element modelling of single-layer folding in elasto-viscous materials: the effect of initial perturbation geometry. Journal of Structural Geology 21, 161–177.

Marti, J., Cundall, P.A., 1982. Mixed discretisation procedure for accurate solution of plasticity problems. International Journal of Numerical Methods and Analytical Methods in Geomechanics 6, 129–139.

Mukhopadhyay, D., 1965. Effects of compression on concentric folds and mechanism of similar folding. Journal of the Geological Society of India 6, 27–41.

Mühlhaus, H.B., Moresi, L.N., Hobbs, B., Dufour, F., 2002. Large amplitude folding in finely layered viscoelastic rock structures. Pure and Applied Geophysics 159, 2311–2333.

Ormand, C.J., Hudleston, P.J., 2003. Strain paths of three small folds from the Appalachian Valley and Ridge, Maryland. Journal of Structural Geology 25, 1841–1854.

Ord, A., 1990. Mechanical controls on dilatant shear zones. In: Knipe, R.J., Rutter, E.H. (Eds.), Deformation Mechanisms, Rheology and Tectonics. Geological Society, London, Special Publications, vol. 54, pp. 183–192.

Passchier, C.W., Druguet, E., 2002. Numerical modeling of asymmetric boudinage. Journal of Structural Geology 24, 1789–1803.

Poliakov, A.N.B., Cundall, P.A., Podladchikov, Y.Y., Lyakhovsky, V.A., 1993. An explicit inertial method for the simulation of viscoelastic flow: an evaluation of elastic effects on diapiric flow in two- and three-layers models. In: Stone, D.B., Runcorn, S.K. (Eds.), Flow and Creep in the Solar System: Observations, Modeling and Theory. Kluwer Academic Publishers, Dordrecht, pp. 175–195.

Ramberg, H., 1961. Relationship between concentric longitudinal strain and concentric shearing strain during folding of homogeneous sheets of rocks. American Journal of Science 259, 382–390.

Ramberg, H., 1964. Selective buckling of composite layers with contrasted rheological properties: a theory for simultaneous formation of several orders of folds. Tectonophysics 6, 307–341.

Ramsay, J.G., 1962. The geometry and mechanics of 'similar' type folds. Journal of Geology 70, 309–327.

Ramsay, J.G., 1967. Folding and Fracturing of Rocks. McGraw-Hill, New York, 568 pp.

Ramsay, J.G., Huber, M.I., 1987. The Techniques of Modern Structural Geology. In: Folds and Fractures, Vol. 2. Academic Press, London, 391 pp.

Schmalholz, S.M., Podladchikov, Y.Y., 2001. Strain and competence contrast estimation from fold shape. Tectonophysics 340, 195–213.

Sherwin, J., Chapple, W.M., 1968. Wavelengths of single layer folds: a comparison between theory and observation. American Journal of Science 266, 167–179.

Shimamoto, T., Hara, I., 1976. Geometry and strain distribution of single-layer folds. Tectonophysics 30, 1–34.

Takeda, Y-T., Griera, A., 2006. Rheological and kinematical responses to flow of two-phase rocks. Tectonophysics 427, 95–113.

Toimil, N.C., 2005. Geometría y patrones de deformación de pliegues simétricos desarrollados en capas competentes. Ph.D. Thesis, University of Oviedo.

Toimil, N.C., Fernández, F.J. Kinematical analysis of symmetrical natural folds developed in competent layers. Journal of Structural Geology, in press. doi:10.1016/j.jsg.2006.10.001.

Treagus, S.H., 1983. A new theory of finite strain variation through contrasting layers, and its bearing on cleavage refraction. Journal of Structural Geology 5, 351–358.

Treagus, S.H., 1988. Strain refraction in layered systems. Journal of Structural Geology 10, 517–527.

Treagus, S.H., 1999. Are viscosity ratios of rocks measurable from cleavage refraction? Journal of Structural Geology 21, 895–901.

Turcotte, D.L., Schubert, G., 1982. Geodynamics—Applications of Continuum Physics to Geological Problems. John Wiley & Sons, New York.

Twiss, R.J., Moores, E.M., 1992. Structural Geology. W.H. Freeman, New York.

Zhang, Y., Hobbs, B.E., Ord, A., Mühlhaus, H.B., 1996. Computer simulation of single-layer buckling. Journal of Structural Geology 18, 643–655.